Published online 7 February 2022

Nucleic Acids Research, 2022, Vol. 50, No. 4 **2211–2222**
https://doi.org/10.1093/nar/gkac043

Mechanistic decoupling of exonuclease III multifunctionality into AP endonuclease and exonuclease activities at the single-residue level

Donghun Lee[1,2,3], Sanghoon Oh[2,4], HyeokJin Cho[1,2,3], Jungmin Yoo[1,2,3] and Gwangrog Lee[1,2,3,4,*]

[1]School of Life Sciences, Gwangju Institute of Science and Technology, Gwangju 61005, Korea, [2]Single-Molecule Biology Laboratory, Gwangju Institute of Science and Technology, Gwangju 61005, Korea, [3]Cell Mechanobiology Laboratory, Gwangju Institute of Science and Technology, Gwangju 61005, Korea and [4]Department of Biomedical Science and Engineering, Gwangju Institute of Science and Technology, Gwangju 61005, Korea

Received September 17, 2021; Revised December 20, 2021; Editorial Decision January 12, 2022; Accepted January 13, 2022

ABSTRACT

Bacterial exonuclease III (ExoIII) is a multifunctional enzyme that uses a single active site to perform two conspicuous activities: (i) apurinic/apyrimidinic (AP)-endonuclease and (ii) 3′→5′ exonuclease activities. The AP endonuclease activity results in AP site incision, while the exonuclease activity results in the continuous excision of 3′ terminal nucleobases to generate a partial duplex for recruiting the downstream DNA polymerase during the base excision repair process (BER). The key determinants of functional selection between the two activities are poorly understood. Here, we use a series of mutational analyses and single-molecule imaging to unravel the pivotal rules governing these endo- and exonuclease activities at the single amino acid level. An aromatic residue, either W212 or F213, recognizes AP sites to allow for the AP endonuclease activity, and the F213 residue also participates in the stabilization of the melted state of the 3′ terminal nucleobases, leading to the catalytically competent state that activates the 3′→5′ exonuclease activity. During exonucleolytic cleavage, the DNA substrate must be maintained as a B-form helix through a series of phosphate-stabilizing residues (R90, Y109, K121 and N153). Our work decouples the AP endonuclease and exonuclease activities of ExoIII and provides insights into how this multifunctional enzyme controls each function at the amino acid level.

GRAPHICAL ABSTRACT

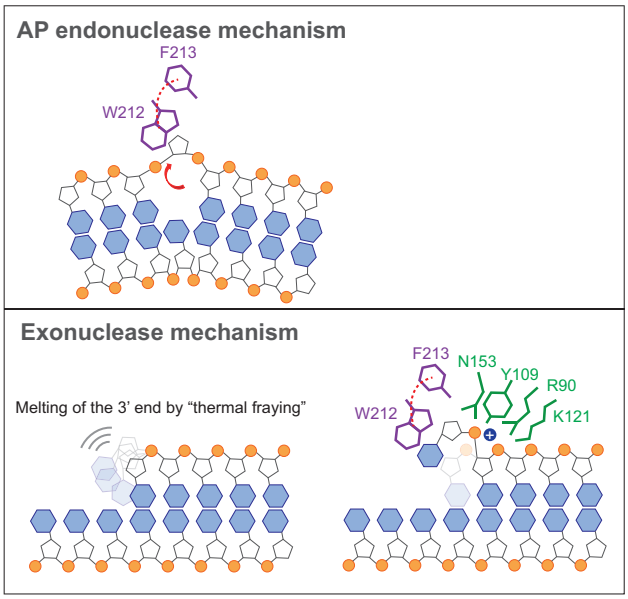

INTRODUCTION

Most endonucleases and exonucleases have evolved as separate enzymes, but some enzymes showing both activities have evolved. For example, human APE1 (1–3) and APE2 (4,5) have functionally evolved into an apurinic/apyrimidinic (AP) endonuclease and exonuclease, respectively, but *Escherichia coli* ExoIII (6) and its bacterial homolog (7–9) are multifunctional nucleases that perform both AP site-specific endonuclease and 3′→5′ exonuclease activities. The multifunctionality of ExoIII occurs at a single active site that specifically recognizes the AP site or 3′ terminal base and then activates endo- and exonuclease activities, depending on the nature of the recognized site.

*To whom correspondence should be addressed. Tel: +82 62 715 3558; Email: glee@gist.ac.kr

During base excision repair (BER) in bacteria, the AP endonuclease performs AP site incision, while the exonuclease continuously excises the 3′ terminal nucleobases and generates a partial duplex to recruit the downstream DNA polymerase for the next step of DNA synthesis (10).

Typically, endonucleases are classified as sequence-specific or nonsequence-specific nucleases (11), while exonucleases are categorized as 3′→5′ or 5′→3′′ exonucleases (12–14), or as processive or distributive nucleases (15–17). The main difference between endo- and exonuclease activities is (i) whether the site to be cut is located outside or inside the DNA substrate and (ii) the ability to cut continuously while translocating along the polymeric axis of the DNA substrate (with so-called enzymatic directionality) (18). The directional movement thus relies on whether the newly generated site acts as the next recognition site to be cut along the polarity of the DNA axis during a series of hydrolysis processes.

Unlike multifunctional enzymes with separate active sites (19–21) (e.g. RecBCD, reverse transcriptase (RT) and DNA polymerase, etc.), the multiple activities of ExoIII rely on a single active site located in one domain (6). An interesting consideration is how multifunctional ExoIII selectively performs the different activities of an AP endonuclease and 3′→5′ exonuclease with one active site in a controllable manner. However, the enzymatic coupling between the two activities involved in functional regulation is poorly understood. Decoupling the molecular mechanisms of the endo- and exonuclease activities in a single active site could open up opportunities to engineer biological enzymatic activity and to develop drugs that target ExoIII in pathogenic bacteria (22). In addition, the human homolog APE1 has been proposed as an early biomarker (23–25) and a promising therapeutic target (26–28) for cancer since its expression level is directly associated with cancer (29–31). Although many studies (6,32,33) have been conducted in an effort to understand the multifunctional activity of wild-type ExoIII, the fundamental understanding of the difference between the AP endonuclease and exonuclease activities of ExoIII remains unknown. Due to the structural and functional similarities of ExoIII to human APE1 and other AP endonucleases (32,34), understanding the mechanism of action of ExoIII may provide insight into the general mechanism of action for both AP endonucleases and exonucleases.

To elucidate the selective determinants for endo- and exonuclease activity, we employed single-molecule imaging and a series of mutational analyses. We found the regulatory mechanism of the endo- and exonuclease activities at a single amino acid level. The aromatic residues near the scissile bond not only function in the recognition of AP sites but also facilitate the formation of a catalytically competent state via the 3′ terminal melting of the substrate. The recognition of AP sites is essential for endonuclease activity, but melting of the 3′ terminus while maintaining an intact B-form helix is a prerequisite for exonuclease activity. Our work deciphers the functional coupling between AP endonuclease and exonuclease activities and provides insights into how the key residues of multifunctional enzymes dictate each function at the amino acid level.

MATERIALS AND METHODS

Protein purification

The *E. coli. ExoIII* gene (wild-type) was cloned into the pB3 vector (6× His tag – TEV – ExoIII gene) by the ligation-independent cloning (LIC) method (35) using SmaI and T4 DNA polymerase and subsequently confirmed by sequencing. All *ExoIII* mutants were obtained by site-directed mutagenesis, and DpnI was used to remove the parent plasmid from the reaction products. After transformation of the vector into BL21-Star (DE3) *E. coli* (Thermo Fisher Scientific), cells were incubated in 1 L LB media (100 μg/ml ampicillin) in a 37°C shaking incubator until the OD_{600} reached 0.6. The culture was incubated for 14∼16 hours in a 16°C shaking incubator after protein induction with a final concentration of 1 mM IPTG. Cells were harvested by centrifugation at 5000 × g for 15 min and resuspended in 50 mL buffer (20 mM Tris–HCl pH 7.5, 250 mM NaCl). Cells were lysed via sonication by repeating 10 s pulse-on and 20 s pulse-off 20 times (total time, 10 min). The cell lysate was centrifuged at 35 000 × g for 30 min to remove insoluble substances. ExoIII was purified using nickel affinity chromatography (His-Trap FF, GE Healthcare). After dialysis in buffer (20 mM Tris–HCl pH 7.5, 250 mM NaCl, 10 mM β-mercaptoethanol), it was concentrated with Centrifugal Filter Devices (Amicon Ultra-15 Centrifugal Filter), aliquoted with 50% glycerol, and stored at –80°C until use.

Cy3 and Cy5 labeling and annealing

All DNA oligonucleotides were purchased from Integrated DNA Technologies (IDT). Amine-modified oligonucleotides were labeled with Cy3-NHS (GE Healthcare) or Cy5-NHS (GE Healthcare) with 5' termini-C6 or Int Amino Modifier C6 dT. The labeled single-stranded DNA (ssDNA) was annealed with its complementary strand in 10 mM Tris–HCl (pH 8.0) with 50 mM NaCl by heating for 3 min at 95°C and cooling slowly to room temperature. Sequence and modification information of the DNA oligos is shown in the supplemental information.

Protein labeling

The 6× glycine N-terminus of ExoIII constructs (D151N, D151N/W212A, D151N/F213A) was obtained through TEV protease cleavage. The labeling reaction was performed in 1× Sortase buffer (50 mM Tris–HCl (pH 7.5), 150 mM NaCl) for 30 min at room temperature with 6x glycine N-terminus of ExoIII constructs, Ca^{2+}-independent sortase, and the Cy3-LPETGG probe (purchased from ANYGEN) at a ratio of 1:2:10. Unreacted free Cy3-LPETGG was removed twice using Micro Bio-Spin™ P-30 Gel Columns in Tris Buffer (RNase-free) (Bio-Rad). To increase the purity, his tag-sortase was removed by passing it through nickel-NTA resin, and Cy3-labeled ExoIII was obtained from the flow-through. Purified Cy3-labeled ExoIII was visualized by 12% SDS-PAGE (ChemiDoc XRS+, Bio-Rad), and the protein concentration and labeling efficiency were measured with a Nanodrop (Thermo Fisher Scientific).

Single-molecule FRET setup and data acquisition

Single-molecule fluorescence resonance energy transfer (smFRET) assays were performed using a prism-type total internal reflection fluorescence (TIRF) setup equipped with an inverted fluorescence microscope (Olympus IX 71) as described previously (36,37). The quartz slides and glass coverslips were coated with polyethylene glycol (biotinylated PEG:mPEG with 1:400 ratio) to prevent nonspecific interactions of DNA and protein with the surface. Fluorescently labeled DNA was immobilized on the PEG-coated surface via the interaction between biotin and neutravidin (Thermo Fisher Scientific). Emission fluorescence signals were separated by a dichroic mirror (630 nm cutoff) and projected onto the EMCCD camera (iXon Ultra 897, Andor). The fluorescence intensities of the donor (Cy3) and acceptor (Cy5) were extracted from the EMCCD camera and amplified by an EM gain function. The Cy3 and Cy5 spots were selected by Gaussian fitting and signal criteria above the average background signal.

The intensities of Cy3 and Cy5 were extracted from the recorded video file by a mapping algorithm compiled in IDL software. The FRET efficiency (E_{FRET}) was calculated by the equation: $E_{FRET} = (I_A - \alpha^* I_D)/(I_A + I_D)$, where α, I_D and I_A are the leakage correction and the donor (Cy3) and acceptor (Cy5) intensities after correction of their background intensity, respectively. smFRET experiments were performed in an imaging buffer containing 50 mM Tris–HCl, pH 7.5, 1 mM $MgCl_2$, 10 mM NaCl, 100 μl/ml BSA, 1 mM DTT and 1 mg/ml Trolox (Sigma-Aldrich) and an oxygen-scavenging system of 1 mg/ml glucose oxidase (Sigma-Aldrich), 0.04% mg/ml catalase (Sigma-Aldrich), and 0.4% (w/v) D-glucose (Sigma-Aldrich). A 532 nm laser (Compass 315M, Coherent) was used to create TIRF illumination after exciting the Cy3 fluorophore, and the fluorescence intensities of Cy3 and Cy5 were simultaneously collected using a water immersion objective (UPlanApo 60×, Olympus). smFRET imaging was recorded with a 100 ms frame-integration time and processed by IDL software. All the data were analyzed using MATLAB and plotted in Origin.

Binding and dissociation assays with smFRET

smFRET experiments were conducted in a flow chamber (38). Three catalytically inactive mutants of ExoIII, D151N (WF), D151N/W212A (AF) and D151N/F213A (WA), were used to examine the binding effect of the aromatic residues at 212 and 213. Cy3-labeled ExoIII mutants (1 nM) were injected into Cy5-labeled DNA substrates (~20 pM) immobilized on the flow chamber at room temperature. All the binding events were obtained with a 100 ms frame-integration time in the imaging buffer. Using MATLAB software, the binding time (on time) and the time taken until binding (off time) in FRET time traces were measured. The mean time (τ) was calculated from histograms of on time and off time by fitting with single-exponential decay. The dissociation constant (K_d) was calculated by $K_d = \frac{\tau_{off} \times [\text{protein concentration}]}{\tau_{on}}$.

Gel-based degradation assays

Assessment of AP-DNA degradation by AP endo- and exonuclease activity. DNA substrates (50 nM) and ExoIII mutants (10 nM) were mixed in 30 μl (Figure 2B, D and E) and 100 μl (Figure 6B) of reaction buffer (50 mM Tris–HCl, pH 7.5, 75 mM NaCl, 10 mM $MgCl_2$, 1 mM DTT). The degradation reaction was carried out at room temperature for various reaction times (0–10 min) and was stopped by adding 1-fold formamide and heating at 95°C. The reaction products were separated through a 20% denaturing PAGE gel (7 M urea) and imaged using a fluorescence imager (ChemiDoc XRS+, Bio-Rad).

Blunt-ended DNA degradation assay by exonuclease activity. DNA substrates and ExoIII mutants were mixed to 50 and 100 nM, respectively, in 30 μl (Figure 3B and C) and 100 μl (Figure 6C) of reaction buffer (50 mM Tris–HCl, pH 7.5, 10 mM NaCl, 10 mM $MgCl_2$, 1 mM DTT). The degradation reaction was carried out at room temperature for 0–10 min and was stopped by adding 1-fold formamide and heating at 95°C. The reaction products were separated with a 20% denaturing PAGE gel (7 M urea) and imaged using a fluorescence imager (ChemiDoc XRS+, Bio-Rad).

Overhang DNA degradation assay. For Figure 4A, DNA substrates (50 nM) and wild-type ExoIII (0.5 nM) were mixed in 100 μl of reaction buffer (50 mM Tris–HCl, pH 7.5, 10 mM NaCl, 10 mM $MgCl_2$, 1 mM DTT). The degradation reaction was carried out at room temperature for 0–10 min and was stopped by adding 1-fold formamide and heating at 95°C. The reaction products were separated with a 20% denaturing PAGE gel (7 M urea) and imaged using a fluorescence imager (ChemiDoc XRS+, Bio-Rad).

In silico reconstitution of a ExoIII–DNA complex

Sequence alignment of ExoIII and APE1 was performed by the VMD program (39) as previously reported (10). Briefly, the 71 conserved residues between ExoIII and APE1 were spatially superimposed, and other residues were aligned based on those conserved residues. We investigated the potential interaction between ExoIII and DNA cocrystallized with APE1 (1) by superimposing the crystal structures of ExoIII (PDB code: 1AKO) and the APE1-DNA complex (PDB code: 1DE8 and 5WN5 for Figures 1A and 6A, respectively). Since the overall secondary structures of ExoIII and APE1 were well matched, ExoIII was loaded onto the DNA substrate by swapping APE1 with ExoIII via structural overlap at the conserved residues. ExoIII–DNA complexes were visualized by UCSF ChimeraX (40,41).

Multiple sequence alignment

The APE1 family (*H. sapiens, B. taurus, M. musculus, D. melanogaster, C. elegans, A. thaliana, S. pneumoniae, N. meningitidis, M. tuberculosis, B. subtilis, P. aeruginosa* and *E. coli*) and protein sequence information of APE2 family (*H. sapiens, R. norvegicus, M. musculus, D. rerio, B. taurus, S. cerevisiae* and *S. pombe*) protein sequence

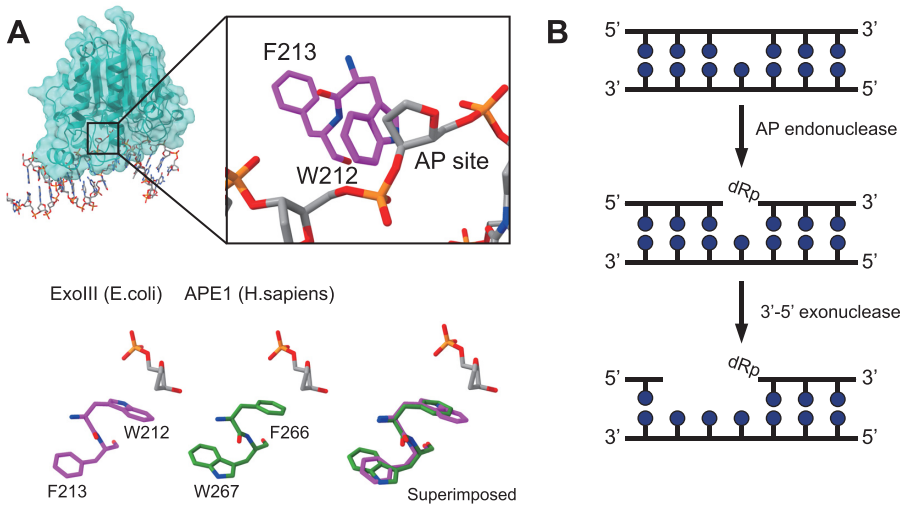

Figure 1. Structure of ExoIII and schematic of the AP endonuclease and 3′-to-5′ exonuclease functions of the enzymes. (**A**) Top: Modeled structure of a DNA–enzyme complex reconstituted *in silico* using ExoIII (PDB entry: 1AKO) (6) and DNA (PDB entry: 1DE8) (1), displaying the recognition of an AP site at which the W212 and F213 aromatic residues stack on the ribose ring. Bottom: Conservation and superimposition of the two aromatic residues at the active site in *E. coli* ExoIII and *human* APE1. (**B**) AP endonuclease and exonuclease functions: ExoIII specifically cuts the AP site on dsDNA and then continues to degrade downstream nucleotides (nt) from the AP site in the 3′-to-5′ direction.

information was obtained from NCBI (https://www.ncbi.nlm.nih.gov/). Multiple sequence alignment was performed with Expresso (a multiple sequence alignment server), an alignment method through structural information and T-Coffee multiple sequence alignment software (http://tcoffee.crg.cat/) available online.

RESULTS

Recognition of the AP site by two aromatic residues and the multiple functions of ExoIII

ExoIII is folded into a four-layered structure in which the two inner layers consist of six-stranded β-sheets and the two outer layers are made of two sets of three and four α-helices, respectively (6). The results of a structural study indicated that ExoIII binds to DNA by contacting the α_M helix with the major groove on the 3′ side of the substrate. The active site is located at the bottom of the valley between the two β-sheets. The polar residues of the active site coordinate a series of ordered water molecules via a hydrogen bond network, permitting a carboxylate in Asp151 to alter its pKa for protonation of the O3′ leaving group, thus triggering a nucleophilic attack on the P-O3′ bond for cleavage (6). The single point mutation D151N of ExoIII makes the enzyme catalytically inactive (10). The catalytic core domain of ExoIII is evolutionarily adopted to higher organisms as the structural framework of AP endonucleases. For example, the human homolog APE1 serves as the main 5′ AP endonuclease in the BER pathway.

Structural and biochemical studies (6,32,42) found that Trp212 at the active site is important for recognizing the AP site due to the aromatic stacking interaction between Trp212 and the sugar ring at the AP site shown in the *in silico* model (10) in Figure 1A. The model was constructed by using the MultiSeq function of VMD (39) and visualized by UCSF ChimeraX (40,41). A similar aromatic stacking interaction was also demonstrated in the sugar stacking of functional RNAs (43). Through site-specific recognition, ExoIII first cleaves the AP site of the DNA substrates and then subsequently degrades the 3′ strand of double-stranded DNA (dsDNA) via exonuclease activity in the 3′-to-5′ direction (Figure 1B). Interestingly, two consecutive aromatic residues, Trp212 and Phe213, are well conserved across all three kingdoms of life, namely, bacteria, archaea and eukaryotes (Supplementary Figure S1). W212 is located close to the AP site, whereas F213 is located one amino acid apart from the AP site. In contrast, only the 213 aromatic residue is conserved in APE2 in eukaryotes, which mainly exhibits exonuclease activity (Supplementary Figure S1). We thus examined the different functions of the two aromatic residues by making enzyme constructs with eight different combinations for the positions, 212 and 213 using Trp and Phe residues (i.e. WF, WW, FF and FW ExoIII possess two consecutive 212 and 213 aromatic rings; WA and FA ExoIII possess only the 212 aromatic residue; and AF and AW ExoIII possess only the 213 aromatic residue.).

One of the two aromatic residues, W212 or F213, is required for AP endonuclease activity

To initiate the AP site-specific cleavage reaction, we constructed a partial duplex substrate with 4 nt ssDNA overhangs at both 3′ ends (top in Figure 2A) since 3′ ssDNA overhangs longer than 4 nt are known to prevent the initiation of exonuclease activity (44). The DNA substrate has an AP site in the middle of the duplex, and a fluorescent dye (Cy5) is attached to the 5′ end of the hydrolyzed strand. This substrate was named AP-DNA. Upon the addition of ExoIII to the AP-DNA in the presence of Mg^{2+}, the reaction begins with the cleavage of dsDNA at the AP site by AP endonuclease and continues to degrade the hydrolyzed strand from the 3′ end in the 3′-to-5′ direction by exonuclease activity (Figure 2A).

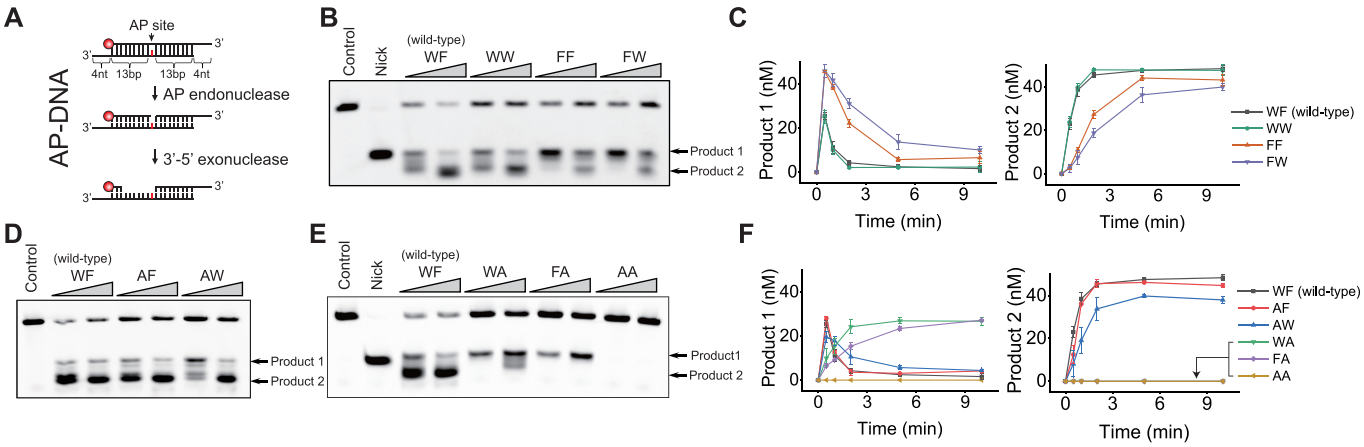

Figure 2. The two consecutive aromatic residues (W212 and F213) in ExoIII participate in the recognition process of the AP site, and at least one of the two is required for AP endonuclease activity. (**A**) Schematic of the DNA substrate (named AP-DNA) used to detect the AP endonuclease and exonuclease activities by an electrophoresis degradation assay. (**B**) Four sets of two aromatic residues at positions 212 and 213 (e.g. WF, WW, FF and FW ExoIII), were used to investigate the effect of each aromatic residue pair on the AP endonuclease and exonuclease activities. Product 1 and product 2 are the products of AP endonuclease and exonuclease, respectively. (**C**) Degradation kinetics of product 1 and product 2 by the four variants used in B. (**D**, **E**) The constructs with only the second aromatic ring (named AF and AW ExoIII) robustly showed both activities, but the constructs with only the 212 aromatic ring (named WA and FA ExoIII) exhibited notable AP endonuclease activity but not exonuclease activity. (**F**) Degradation kinetics of product 1 and product 2 by the six variants used in D and E. For experimental conditions, 5 nM (C and F) and 10 nM (B, D and E) proteins were used in the presence of 10 mM $MgCl_2$.

Although a previous study showed that the F213W mutant (i.e. WW ExoIII in *B. subtilis* of Supplementary Figure S1) retains its AP endonuclease activity (45), other combination mutants have not been investigated. Therefore, we tested four constructs with different combinations of the two aromatic residues at the 212 and 213 positions in the vicinity of the active site (i.e. WF, WW, FF and FW ExoIII). All of their reactions resulted in cleavage at the AP site (product 1 in Figures 2B, left of C and Supplementary Figure S2) and a series of subsequent digestions due to exonuclease activity (product 2 in Figures 2B, right of C and Supplementary Figure S2). The results suggested that the type of aromatic rings at both positions was not critical for the two activities if two aromatic rings were present. To further differentiate the effect of each position, either W212 or F213 was mutated to an alanine residue. Strikingly, both AF and AW ExoIII (i.e. the constructs with only the 213 aromatic ring) showed robust AP endo- and exonuclease activities (Figures 2D, F and Supplementary Figure S2). WA and FA ExoIII (i.e. the constructs with only the 212 aromatic ring) exhibited notable AP endonuclease activity but significantly reduced exonuclease activity (i.e. ∼82.5% and ∼100% reduction in product 2 for WA and FA ExoIII, respectively, compared to the wild-type ExoIII) (Figures 2E, F and Supplementary Figure S2). The relative AP endonuclease activity with AP-DNA was as follows: wild-type ExoIII, the constructs with only the 213 aromatic ring, and the constructs with only the 212 aromatic ring (i.e. WF, AF and WA ExoIII in Supplementary Figure S3).

The F213 aromatic residue plays an important role in exonuclease activity

To evaluate exonuclease activity on only one side of both 3′ ends, we used a unilateral blunt-ended substrate, in which the hydrolysable strand was labeled with Cy5 at the 5′ end and the complementary strand was extended by 5 nt ssDNA from the 3′ end opposite to Cy5 to prevent the initiation of exonuclease activity (Figure 3A). This DNA substrate was named blunt-ended DNA. The constructs with two rings (i.e. WF, WW, FF and FW ExoIII) all showed 3′→5′ exonuclease activity (Figure 3B), but with different degrees of activity (Figures 3B, D, Supplementary Figures S4A and C). In contrast, the constructs with only the 213 ring (i.e. AF and AW ExoIII) showed exonuclease activity, but the constructs with only the 212 ring (i.e. WA and FA ExoIII) did not exhibit notable exonuclease activity on the blunt-ended DNA (Figures 3C, Supplementary Figures S4B and D). The time course assay of degradation revealed that the constructs with only the 213 ring (i.e. AF and AW ExoIII) possess much stronger exonuclease activity than wild-type ExoIII (Figures 3E, F–I, and Supplementary Figure S4C). In addition, alanine mutations at positions 212 and 213 (i.e. AA ExoIII) completely abolished AP endonuclease activity (the last two lanes in Figure 2E) and exonuclease activity (last lane in Figures 3C and Supplementary Figure S4D). The spurious band (fifth lane) in Figure 3C turned out to be due to weak degradation of the blunt-ended DNA by 100 nM WA ExoIII (Supplementary Figure S4B). We also found that the WA ExoIII has weak exonucleolytic activity at a high enzyme concentration of 100 nM (Figures 3C and Supplementary Figure S4B) but not at 50 nM (Supplementary Figure S4D). Overall, the constructs with only the 213 ring (AF and AW ExoIII) possessed both AP endo- and exonuclease activities (Figures 2D and 3C), whereas the constructs with only the 212 ring (WA and FA ExoIII) possessed only AP endonuclease activity (Figures 2E and 3C), indicating that the 213 aromatic residue is essential for exonuclease activity.

The melting of the 3′ terminal base pair must occur prior to cleavage

Next, we evaluated whether the melting of the 3′ terminal nucleotides occurs before or after cleavage during exonucle-

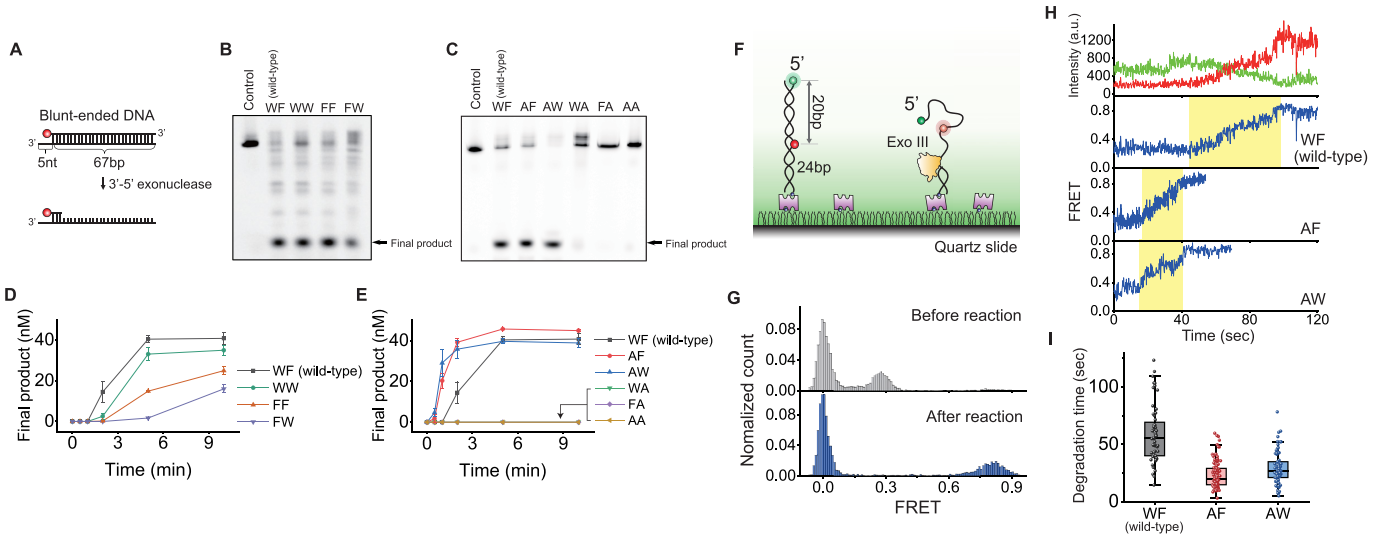

Figure 3. The second aromatic residue (F213) is indispensable for exonuclease activity. (**A**) Schematic of the DNA substrate (named blunt-ended DNA) with a 5 nt ssDNA extension from the 3′ end opposite to Cy5 for the gel electrophoresis degradation assay. (**B**) The constructs with the four combinations of aromatic residues at positions 212 and 213 (i.e. WF, WW, FF and FW ExoIII) were used to investigate the effect of each aromatic residue set on exonuclease activity. (**C**) The constructs with only the second aromatic ring (AF and AW ExoIII) showed both AP endonuclease and exonuclease activities, but the constructs with only the 212 aromatic ring (WA and FA ExoIII) exhibited only AP endonuclease activity, without any notable exonuclease activity. (D, E) Degradation kinetics of blunt-ended DNA by the ExoIII variants as in B (**D**) and as in C (**E**). (F–I) Single-molecule degradation assay using blunt-ended DNA and the wild-type WF, AF or AW ExoIII variants. (**F**) Schematics of the smFRET assay for measuring blunt-end DNA degradation by ExoIII variants (WF AF and AW). Cy3 was labeled at the 5′ end of the nondegraded strand, and Cy5 is placed 20 bp away from Cy3. (**G**) smFRET histograms before (gray) and after a 3-min reaction (blue). (**H**) A representative FRET time trajectory with 40 nM ExoIII variants (wild-type, AF and AW) and 10 mM $MgCl_2$. The yellow boxes show how the degradation time was measured. Green and red curves represent the donor and acceptor intensities, respectively, and the blue curve represents the calculated FRET efficiency. (**I**) Degradation times with ExoIII variants (wild-type, AF and AW): wild-type, 58.8 ± 3.30 s; AF, 26.2 ± 1.52 s; AW, 29.3 ± 1.63 s (mean ± SEM). 10 mM Mg^{2+} and 50 nM ExoIII variants were used for degradation gel assay. 10 mM Mg^{2+} and 40 nM ExoIII variants were used for smFRET assay. For experimental conditions, 100 nM (B and C), 50 nM (D and E) and 40 nM (F–I) proteins were used in the presence of 10 mM $MgCl_2$.

olytic degradation. Gel-based degradation assays were performed on partial duplexes at concentrations as low as 0.5 nM ExoIII (wild-type) to slow down degradation and discriminate differences in degradation rates (Figures 4A and Supplementary Figure S5). To further evaluate the above process, three partial duplexes were created with 0, 1 and 2 mismatches (M) at the 3′ end of the ssDNA–dsDNA (ss–ds) junction (Figure 4A, named 5′OPD, 5′OPD-1M and 5′OPD-2M, respectively). The results showed that the degradation of 5′OPD-1M was faster than those of 5′OPD and 5′OPD-2M (Figure 4A), suggesting that 5′OPD-1M, which underwent a premelting step prior to cleavage, is favorable for degradation. Taken together, the results show that the melting of the 3′ terminal base pair must occur prior to exonucleolytic cleavage, suggesting that the premelted 3′ end is not only a catalytically competent state but also an intermediate state before cleavage in the reaction coordinate.

To understand the difference in the degradation of 5′OPD variants with and without mismatches by ExoIII, we used a smFRET technique (Figure 4B). In single molecule assays, a catalytic D151N mutant (10) was used to prevent DNA cleavage during the measurements (Supplementary Figure S6). In a control experiment, it was confirmed that the D151N ExoIII has a similar binding affinity to that of the wild-type ExoIII by EMSA (Supplementary Figure S7). The three partial duplexes were labeled 6 nt inside the duplex on the nonhydrolyzed complementary strand with a FRET acceptor, Cy5 (named Cy5-labeled 5′OPD variants), and ExoIII was labeled with a FRET donor, Cy3 (named Cy3-labeled ExoIII), at the N-terminus via site-specific labeling by sortase (46). The FRET-time trajectories obtained from the partial duplexes with 0, 1 and 2 mismatches at the 3′-end of the ss–ds junction (Figure 4C) showed different binding and dissociation kinetics (Figure 4C) and FRET values (Figure 4D). Histograms (Figure 4E) were prepared using binding (t_{off}) and dissociation (t_{on}) times measured from FRET-time trajectories and were fitted to single exponential decay ($y = e^{-t/\tau}$) to obtain characteristic decay times of τ_{off} and τ_{on}. K_d then was calculated as in Supplementary Figure S8E (47). The comparison of binding affinities (dissociation constant, K_d) in the presence of 1 mM $MgCl_2$ for the 5′OPD variants revealed that ExoIII binds more tightly to 5′OPD-1M than to 5′OPD and 5′OPD-2M by 2.6-fold and 138-fold, respectively (Figure 4F). This affinity tendency is also remained even at a higher $MgCl_2$ concentration of 10 mM (Supplementary Figure S8). Overall, the 3′ single terminal melting at the ss–ds junction provides higher affinity for ExoIII to firmly cleave the 3′ terminal bases.

The sequence selectivity of ExoIII has been reported for dsDNA with a 5′ ssDNA overhang (48) and for the blunt-ended DNA (49), but the mechanism of the melting capability by ExoIII is not well understood. We tested whether the removal of the 3′-terminal nucleotide requires induced melting of the 3′-terminal pair. We compared the rates of DNA degradation by 3′-terminal stability using 3′OPDs with C:G

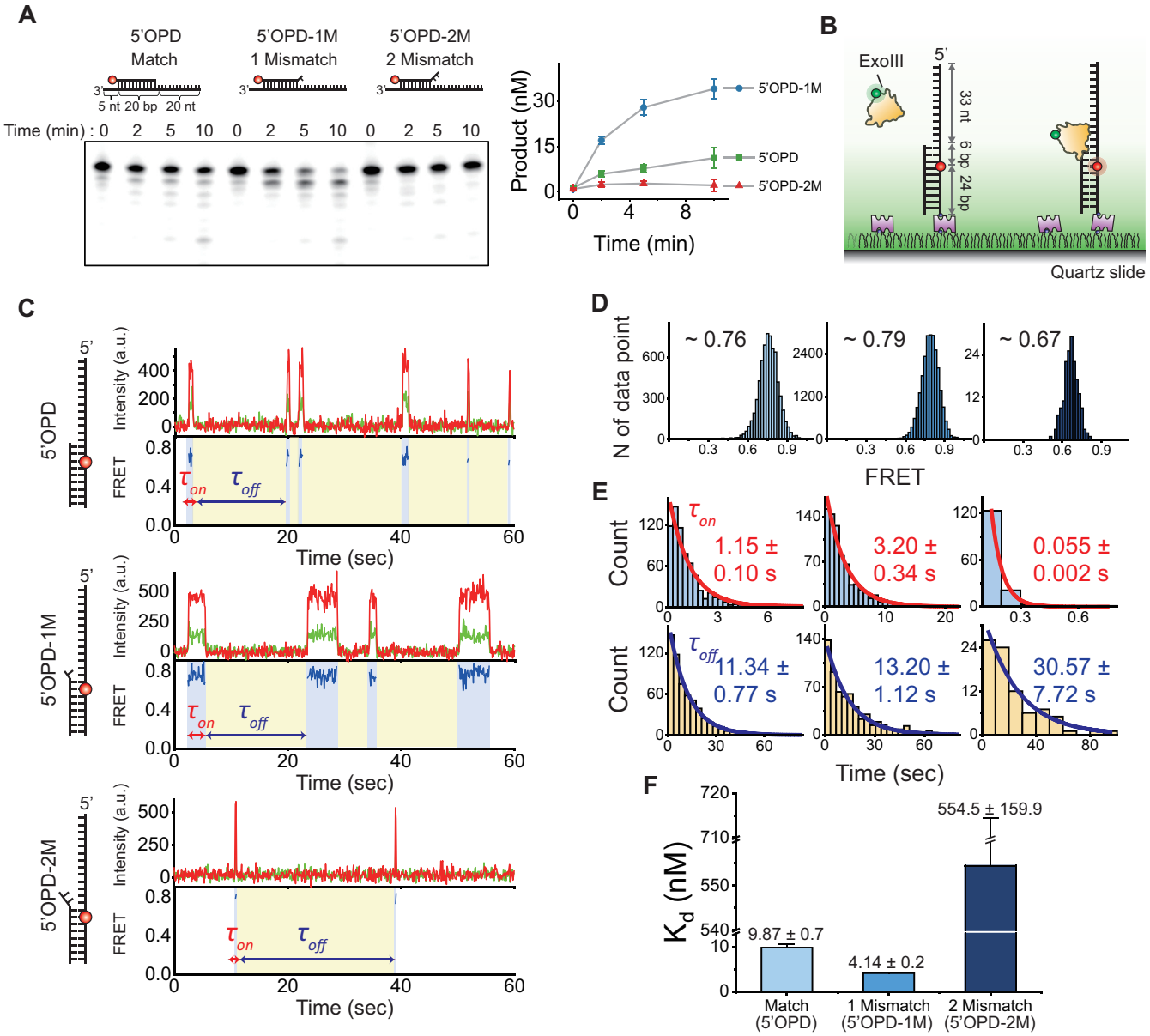

Figure 4. The melting of 3′ terminal nucleotides prior to cleavage is a catalytically competent state and essential intermediate required for the exonucleolytic degradation catalyzed by ExoIII. (**A**) The degradation of 5′OPD-1M is faster than that of 5′OPD and 5′OPD-2M, suggesting that melting of the 3′ terminal base pair must occur prior to cleavage. (**B**) Experimental schematic before (left) and after (right) binding to the Cy5-labeled DNA substrate by Cy3-labeled ExoIII. (**C**) Representative FRET-time trajectories showing the binding events of ExoIII to three DNA substrates: 5′OPD (top), 5′OPD-1M (middle) and 5′OPD-2M (bottom) in the presence of 1 mM $MgCl_2$ (also see 10 mM $MgCl_2$ in Supplementary Figure S8). (D, E) Histograms of FRET (97 170 and 298 traces were used to build FRET histograms of 5′OPD, 5′OPD-1M and 5′OPD-2M, respectively) (**D**) and binding and dissociation times (**E**) for 5′OPD (left), 5′OPD-1M (middle) and 5′OPD-2M (right). (**F**) Binding affinity (dissociation constant, K_d). K_d was calculated as $K_d = k_{off}/k_{on}$, where k_{off} and k_{on} are obtained from single-exponential decay fitting on the distributions of binding and dissociation times. For experimental conditions, 1 nM Cy3-labeled ExoIII(D151N) in the presence of 1 mM $MgCl_2$ was used with the time-resolution of 100 ms for smFRET assays (B–F). Due to weaker affinity in the presence of 10 mM $MgCl_2$, different concentrations of Cy3-labeled D151N ExoIII (5 nM protein for 5′OPD and 5′OPD-1M and 20 nM protein for 5′OPD-2M) were used with the time-resolution of 50 ms for smFRET assays (see Supplementary Figure S8).

or C:I at the 3′ terminal pair of the ss–ds junction (Supplementary Figure S9A). If the induced melting is required, the weaker pair (i.e. C:I) should be degraded faster. The stability dependence in the degradation kinetics (Supplementary Figure S9B) suggested that the 3′ terminal melting is indeed required for the removal of 3′-terminal nucleotides. Based on the crystal structure, highly conserved Y215 near the 3′ terminal pair at the ss–ds junction was a good candidate to serve as a wedge that can be used to unstack the 3′ terminal nucleotide (Supplementary Figure S10A). We tested the exonucleolytic activity of the Y215A mutant (Supplementary Figure S10A) for AP-DNA (Supplementary Figure S10B) and blunt-ended DNA (Supplementary Figure S10D). Consequently, the Y215A mutation reduced the exonucleolytic activity for AP-DNA but completely abolished it for blunt-ended DNA (see product 2 for AP-DNA in

Supplementary Figure S10B-C and final product for blunt-ended DNA in Supplementary Figure S10D, E). This data suggests that Y215 is to some extent involved in the unstacking of the 3′-terminal nucleotide.

F213 stabilizes the melted state of the 3′ end of the hydrolysable strand

The aromatic residues at the two positions, 212 and 213, are important for the recognition of AP sites (Figure 2), but their effect on exonuclease activity is unknown. In particular, the removal of the 213 aromatic residue, entirely abolishes exonuclease activity (last three lanes in Figure 3C). In addition, close examination of the *in silico* structure (Figure 1A) suggested that F213 could interact to stabilize the 3′ terminal nucleotides opened by the melting or fraying. We thus hypothesized that F213, which is in the vicinity of the ss-ds junction, might be involved in the stabilization of the melted 3′ terminal nucleotides during exonuclease activity. If this hypothesis is true, the binding affinity of AF ExoIII to 5′OPD-1M would be higher than that of other mutants to 5′OPD-1M.

To test this hypothesis, we measured the binding affinity of the constructs with only the 212 ring (WA/D151N ExoIII) and only the 213 ring (AF/D151N ExoIII) to 5′OPD-1M by a single-molecule binding assay. The fluorescent labeling scheme for measurements was the same as that in Figure 4B. Representative smFRET trajectories of AF/D151N ExoIII and WA/D151N ExoIII showed that the time bound to 5′OPD-1M was longer than that bound to 5′OPD (Figure 5A and B). Consistently, the difference in K_d between 5′OPD-1M and 5′OPD at the 3′ end of the ss-ds junction was ∼7-fold for AF ExoIII (Figures 5C and Supplementary Figure S11) and ∼3.1-fold for WA ExoIII (Figures 5D and Supplementary Figure S11). The affinity of the AF ExoIII to intact 5′OPD was ∼8.7 times stronger than that of the WA construct (Figure 5E), whereas it was ∼2.5 times higher than that of the WF construct (wild-type). In contrast, the affinity of the AF ExoIII for 5′ OPD-1M, representing a catalytically competent intermediate state, was ∼20 times higher than that of the WA ExoIII (Figures 5E and Supplementary Figure S11), whereas it was ∼7 times stronger than that of the WF ExoIII (wild-type). The higher affinity of AF ExoIII suggests that indeed, the 3′ end is stabilized by the F213 aromatic residue, upon thermal melting of the 3′ end. In contrast, the AA mutant showed a K_d value of ∼1.3 μM with 5′OPD-1M, which was more than ∼3 orders of magnitude lower than the AF mutant with a K_d value of ∼0.58 nM (green in Figure 5E and Supplementary Figure S12).

For the 3′ end to remain melted prior to cleavage, the DNA substrate is further stabilized via phosphate-interacting residues

The fact that the 2 nt premelted 5′OPD-2M was poorly degraded by ExoIII compared to 5′OPD-1M and 5′OPD (Figure 4A) indicates that the second phosphate after the 3′ terminal base should remain at the positions of the B-form helix of the duplex. An *in silico* model of ExoIII (Figure 6A) suggested that a series of amino acid residues (i.e. R90, Y109, K121 and N153) could interact with and stabilize the first and second phosphates during the melting process of the 3′ terminal bases. The four protein residues were thus mutated to alanine, and the effect of these mutations on AP endonuclease and exonuclease activity was tested.

All four ExoIII mutants exhibited AP endonuclease activity against AP-DNA (Figure 6B and Supplementary Figure S13) but did not show exonuclease activity against blunt-ended DNA (Figure 6B, C and Supplementary Figure S13). Overall, the data suggested that the melting of the 3′ terminal nucleotides should precede cleavage, while the position of the second phosphate or the positions of both the first and second phosphates remain within the B-form helix of the duplex. The fact that all the phosphate-stabilizing residues (i.e. R90, Y109, K121 and N153) were indispensable for exonuclease activity indicated that the 1 nt melting of the 3′ end is a key intermediate leading to the catalytically competent state for cleavage.

The mechanistic model of multifunctional ExoIII with AP endo- and exonuclease activity

At least one of two aromatic residues (W212 or F213) is needed for AP endonuclease activity. In the absence of both aromatic residues, ExoIII cannot cleave AP sites as an AP endonuclease and cannot degrade the 3′ strands of dsDNA as an exonuclease (last lanes in Figures 2E and 3C). However, when the 212 aromatic residue alone (i.e. WA and FA) is present, ExoIII acts as an AP endonuclease but not as an exonuclease (Figures 2E, F, 3C, E, and Supplementary Figure S4), whereas when the F213 aromatic residue alone (i.e. AW and AF) is present, ExoIII functions as both an AP endonuclease and an exonuclease (Figures 2D, F, 3C and E).

In our model (Figure 7), the first and second aromatic residues at positions 212 and 213 participate in the recognition of AP sites (left of Figure 7A), whereas the aromatic residue at 213 participates in not only the recognition of the AP site for AP endonuclease activity but also the stabilization of the 3′ terminal melting at the ss–ds junction for exonuclease activity (Figure 7B). For exonuclease activity, melting of the 3′ end is a prerequisite as a catalytically competent intermediate state that facilitates exonucleolytic cleavage (Figure 7B). The melted state of the 3′ end by thermal or induced fraying should be stabilized by the F213 aromatic residue regardless of the presence of the first aromatic residue (W212), and the B-form helix of the partial duplex except the 3′ terminal should be stabilized by a series of phosphate-stabilizing residues (R90, Y109, K121 and N153) for exonuclease activity (right of Figure 7A).

DISCUSSION

Here, we aimed to identify which residues of ExoIII, which has one active site, control the multifunctional AP endonuclease and 3′→5′ exonuclease enzymatic activities of this enzyme. Given the cleavage ability of this enzyme, the key to controlling the multifunctional activity at the amino acid level is (i) the presence of two residues W212 and F213 at the AP site to allow redundancy in the case of the mutation of one of the two residues and (ii) stable retention of the 3′ melted state as a catalytically competent state by

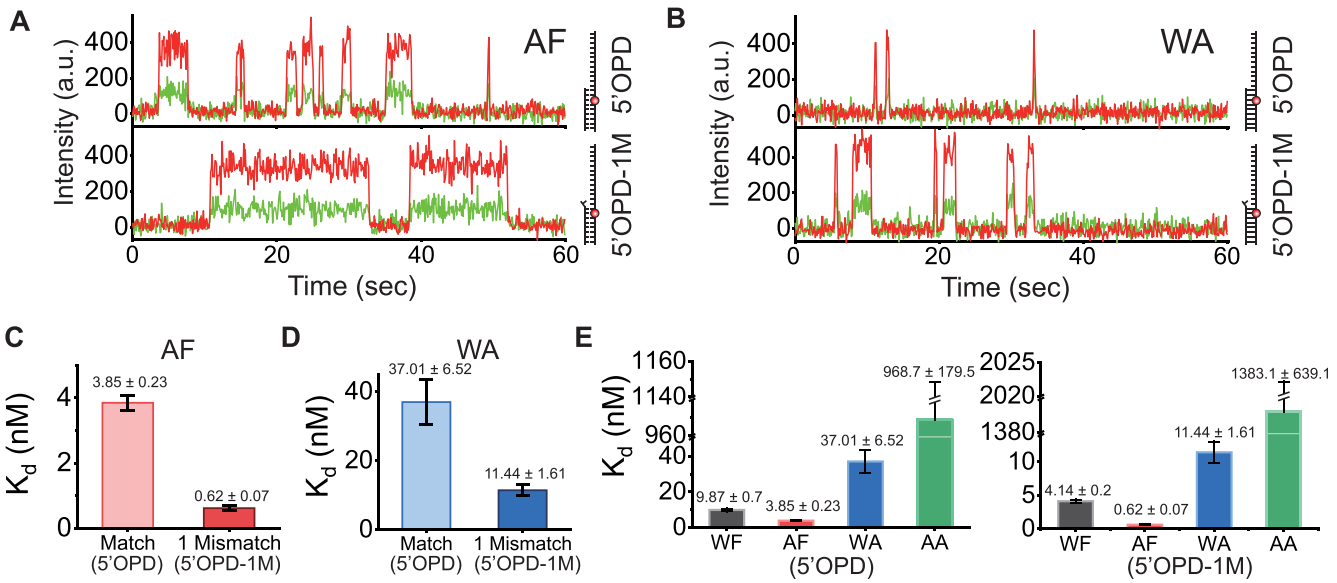

Figure 5. The aromatic residue F213 in the vicinity of the ssDNA–dsDNA junction is involved in the stabilization of the melted 3′ terminal nucleotides during exonuclease activity. (A, B) Representative FRET-time trajectories for AF ExoIII (**A**) and WA ExoIII (**B**). (C, D) Comparison of K_d of 5′OPD and 5′OPD-1M for AF ExoIII (**C**) and WA ExoIII (**D**). (**E**) Comparison of K_d of WF, AF, WA and AA ExoIII on 5′OPD (left) and 5′OPD-1M (right). The higher affinity of AF ExoIII suggested that the 3′ end is stabilized by the second aromatic residue, F213, upon the melting of the 3′ end. Experimental conditions were the same as in Figure 4.

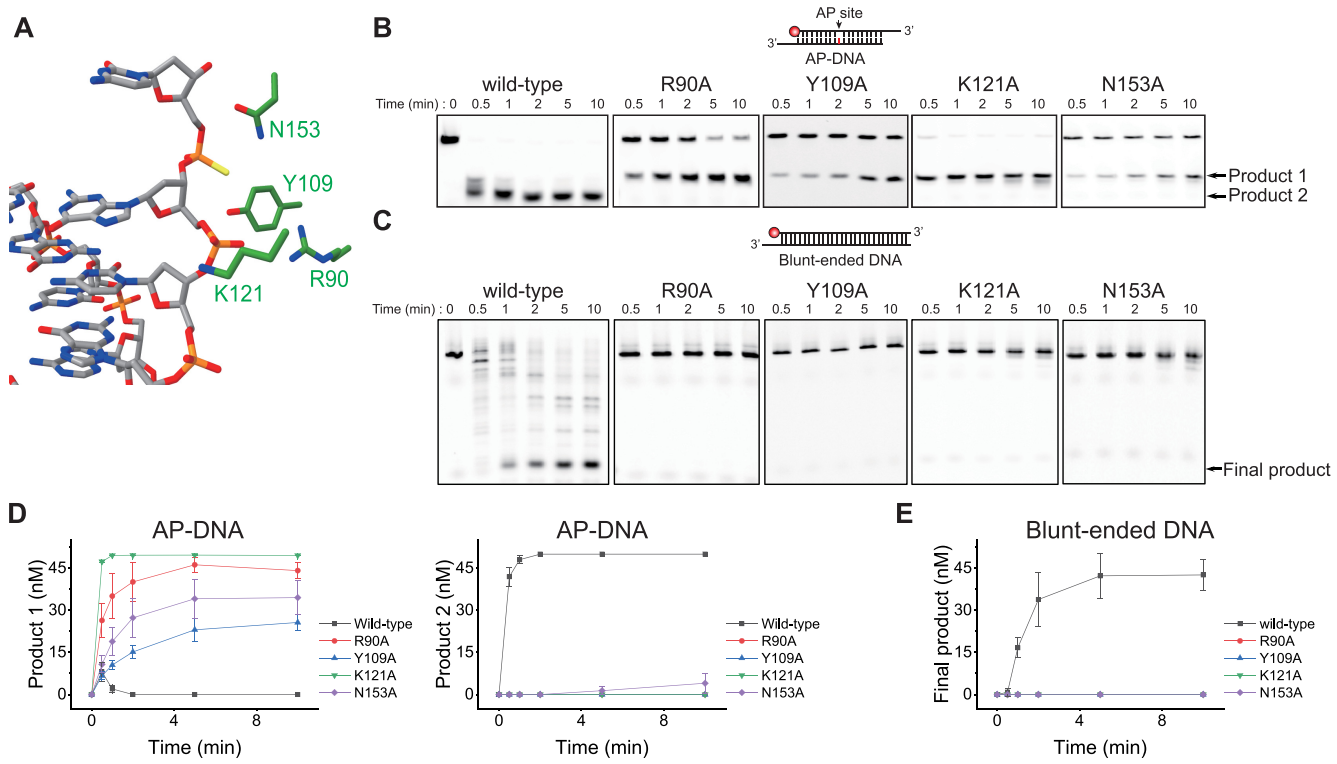

Figure 6. DNA-binding residues (R90, Y109, K121, N153) interact with and stabilize the second phosphate to keep the DNA duplex in a B-form helix while maintaining the melting of the 3′ terminal bases. (**A**) *In silico* model of ExoIII showing phosphate-interacting residues (green). (B, C) Assessment of AP-DNA (**B**) and blunt-ended DNA (**C**) degradation by four single amino acid mutants of ExoIII with the electrophoresis degradation assay. The mutation of one of the four residues to alanine, which stabilizes the first and second phosphates along the DNA backbone near the B-form DNA helix, abolishes exonuclease activity but not AP endonuclease activity, indicating that the 3′ end melted state is a key intermediate leading to the catalytically competent state for exonucleolytic cleavage. (D, E) Degradation kinetics of AP-DNA (**D**) and blunt-ended DNA (**E**) by the ExoIII variants. For experimental conditions, 10 nM (B) and 100 nM proteins (C) were used in the presence of 10 mM $MgCl_2$.

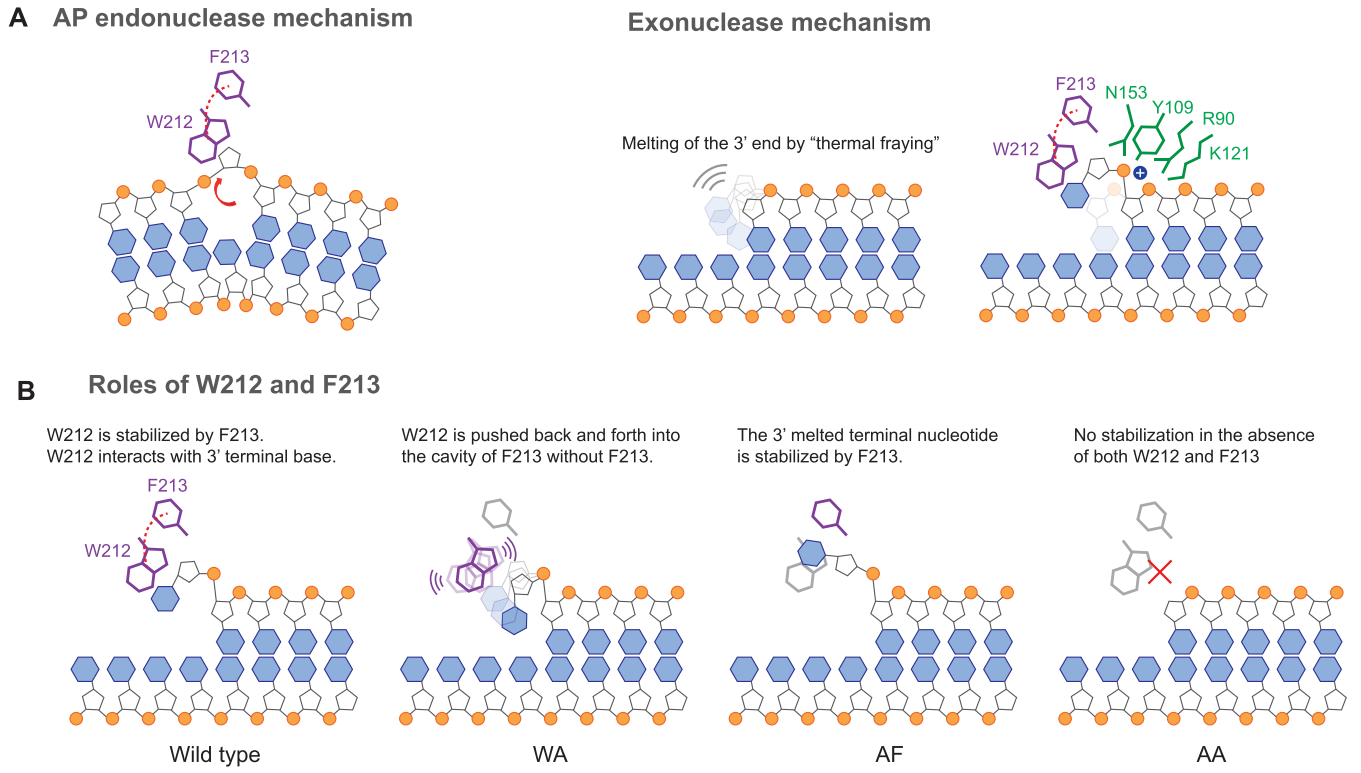

Figure 7. Model of multifunctional ExoIII with AP endonuclease and 3′-to-5′ exonuclease activity. (**A**) For AP endonuclease activity (left), at least one of two aromatic residues (W212 or F123) is needed. For exonuclease activity (right), melting of the 3′ end is a prerequisite as a catalytically competent intermediate state that facilitates exonucleolytic cleavage. The melted state of the 3′ end by thermal or induced fraying should be stabilized by the first and second aromatic residues (W212 and F213), and the B-form helix of the partial duplex, while the 3′ terminal should be stabilized by a series of phosphate-stabilizing residues (R90, Y109, K121 and N153) for exonuclease activity. (**B**) When only the 212 aromatic residue (W212) is present, as in WA ExoIII, only AP endonuclease activity occurs, whereas when only the second aromatic residue (F213) is present, as in AF ExoIII, both AP endonuclease and exonuclease activities occur, suggesting that F213 is essential for exonuclease activity.

F213, providing additional time for ExoIII to cleave the 3′ end. The fact that the two aromatic residues were very well conserved among species, as shown in the protein sequence analysis (Supplementary Figure S1), showed that they are evolutionarily important for AP endo- and exonuclease activities. In short, the F213 (second aromatic residue) not only serve as a 'spare-tire' of endo-activity (Figure 2D) when the W212 (first aromatic residue) is mutated to nonaromatic residues (see successive aromatic residues in purple in Supplementary Figure S1) but also plays a key role in exo-activity (third and fourth lanes in Figure 3C).

By understanding the mechanism of multifunctionality within a single active site, we can provide opportunities to engineer biological enzymatic activity. We successfully engineered the multiple functions of ExoIII either to result in AP endonuclease activity alone or to improve exonuclease activity. First, to induce AP endonuclease activity alone, similar to human APE1, one of the key residues for exonuclease activity (i.e. F213, R90, Y109, K121 and N153) was mutated to prevent the stabilization of the exonucleolytic melted state of the 3′ end. As a result, all of the mutants showed robust AP endonuclease activity but not exonuclease activity. Second, by removing the 212 aromatic residue at position 212, the AF and AW mutants became more efficient exonucleases than wild-type ExoIII (Figure 3D), suggesting that the mutants with only the second aromatic ring may stabilize the 3′ melted terminal bases better than wild-type ExoIII.

In conclusion, we elucidated the mechanism of ExoIII and decoupled its multifunctional activity at single amino acid resolution. We found that, regardless of the type, at least one of the two aromatic residues, W212 or F213, is essential for AP endonuclease activity, whereas the second residue, F213, participates in the stabilization of the melted state of the 3′ end to form a catalytically competent state for exonuclease activity. We also found that maintaining the second phosphate positions in the B-form helix along with the melted 3′ end is also important to provide enough time for ExoIII to cleave the 3′ end of the hydrolysable strand.

DATA AVAILABILITY

The data that support the findings of this study are available from the corresponding author upon reasonable request.

SUPPLEMENTARY DATA

Supplementary Data are available at NAR Online.

ACKNOWLEDGEMENTS

We thank all Lee's laboratory members and J. Yoo for experimental help and valuable inputs. Molecular graphics were prepared with UCSF ChimeraX.

FUNDING

GIST Research Institute (GRI); National Research Foundation of Korea (NRF) grant funded by the Korean government [NRF-2020R1A2C2006712, NRF-2019R1A4A1028802]; Korean Health Technology R&D Project; Ministry of Health and Welfare, Republic of Korea [HA17C0031: #1720050]. Funding for open access charge: National Research Foundation of Korea [NRF].
Conflict of interest statement. None declared.

REFERENCES

1. Mol,C.D., Izumi,T., Mitra,S. and Talner,J.A. (2000) DNA-bound structures and mutants reveal abasic DNA binding by APE1 DNA repair and coordination. *Nature*., **403**, 451–456.
2. Freudenthal,B.D., Beard,W.A., Cuneo,M.J., Dyrkheeva,N.S. and Wilson,S.H. (2015) Capturing snapshots of APE1 processing DNA damage. *Nat. Struct. Mol. Biol.*, **22**, 924–931.
3. Whitaker,A.M., Flynn,T.S. and Freudenthal,B.D. (2018) Molecular snapshots of APE1 proofreading mismatches and removing DNA damage. *Nat. Commun.*, **9**, 399.
4. Hadi,M.Z., Ginalski,K., Nguyen,L.H. and Wilson,D.M. 3rd. (2002) Determinants in nuclease specificity of ape1 and ape2, human homologues of escherichia coli exonuclease III. *J. Mol. Biol.*, **316**, 853–866.
5. Burkovics,P., Szukacsov,V., Unk,I. and Haracska,L. (2006) Human ape2 protein has a 3′-5′ exonuclease activity that acts preferentially on mismatched base pairs. *Nucleic Acids Res.*, **34**, 2508–2515.
6. Mol,C.D., Kuo,C.F., Thayer,M.M., Cunningham,R.P. and Tainer,J.A. (1995) Structure and function of the multifunctional DNA-repair enzyme exonuclease III. *Nature*, **374**, 381–386.
7. Georg,J., Schomacher,L., Chong,J.P.J., Majerník,A.I., Raabe,M., Urlaub,H., Müller,S., Ciirdaeva,E., Kramer,W. and Fritz,H.J. (2006) The methanothermobacter thermautotrophicus ExoIII homologue mth212 is a DNA uridine endonuclease. *Nucleic Acids Res.*, **34**, 5325–5336.
8. Lakomek,K., Dickmanns,A., Ciirdaeva,E., Schomacher,L. and Ficner,R. (2010) Crystal structure analysis of DNA uridine endonuclease mth212 bound to DNA. *J. Mol. Biol.*, **399**, 604–617.
9. Silhan,J., Nagorska,K., Zhao,Q., Jensen,K., Freemont,P.S., Tang,C.M. and Baldwin,G.S. (2012) Specialization of an exonuclease III family enzyme in the repair of 3′ DNA lesions during base excision repair in the human pathogen neisseria meningitidis. *Nucleic Acids Res.*, **40**, 2065–2075.
10. Yoo,J., Lee,D., Im,H., Ji,S., Oh,S., Shin,M., Park,D. and Lee,G. (2021) The mechanism of gap creation by a multifunctional nuclease during base excision repair. *Sci. Adv.*, **7**, eabg0076.
11. Yang,W. (2011) Nucleases: diversity of structure, function and mechanism. *Q. Rev. Biophys.*, **44**, 1–93.
12. Ceska,T.A., Sayers,J.R., Stier,G. and Suck,D. (1996) A helical arch allowing single-stranded DNA to thread through T5 5′-exonuclease. *Nature*, **382**, 90–93.
13. Shevelev,I.V. and Hübscher,U. (2002) The 3′-5′ exonucleases. *Nat. Rev. Mol. Cell Biol.*, **3**, 364–375.
14. Orans,J., McSweeney,E.A., Iyer,R.R., Hast,M.A., Hellinga,H.W., Modrich,P. and Beese,L.S. (2011) Structures of human exonuclease 1 DNA complexes suggest a unified mechanism for nuclease family. *Cell*, **145**, 212–223.
15. Thomas,K.R. and Olivera,B.M. (1978) Processivity of DNA exonucleases. *J. Biol. Chem.*, **253**, 424–429.
16. Lee,G., Bratkowski,M.A., Ding,F., Ke,A. and Ha,T. (2012) Elastic coupling between RNA degradation and unwinding by an exoribonuclease. *Science*, **336**, 1726–1729.
17. Wang,T., Sun,H.L., Cheng,F., Zhang,X.E., Bi,L. and Jiang,T. (2013) Recognition and processing of double-stranded DNA by ExoX, a distributive 3′-5′ exonuclease. *Nucleic. Acids. Res.*, **41**, 7556–7565.
18. Singleton,M.R., Dillingham,M.S. and Wigley,D.B. (2007) Structure and mechanism of helicase and nucleic acid translocates. *Annu. Rev. Biochem.*, **76**, 23–50.
19. Singleton,M.R., Dillingham,M.S., Gaudier,M., Kowalczykowski,S.C. and Wigley,D.B. (2004) Crystal structure of RecBCD enzyme reveals a machine for processing DNA breaks. *Nature*, **432**, 187–193.
20. Kohlstaedt,L.A., Wang,J., Friedman,J.M., Rice,P.A. and Steitz,T.A. (1992) Crystal structure at 3.5 Å resolution of HIV-1 reverse transcriptase complexed with an inhibitor. *Science*, **256**, 1783–1790.
21. Biertümpfel,C., Zhao,Y., Kondo,Y., Ramón-Maiques,S., Gregory,M., Lee,J.Y., Masutani,C., Lehmann,A.R., Hanaoka,F. and Yang,W. (2010) Structure and mechanism of human DNA polymerase. *Nature*, **465**, 1044–1048.
22. Kurthkoti,K., Kumar,P., Sang,P.B. and Varshney,U. (2020) Base excision repair pathways of bacteria: new promise for an old problem. *Future Med. Chem.*, **12**, 339–355.
23. Shin,J.H., Choi,S., Lee,Y.R., Park,M.S., Na,Y.G., Irani,K., Lee,S.D., Park,J.B., Kim,J.M., Lim,J.S. *et al.* (2015) APE1/ref-1 as a serological biomarker for the detection of bladder cancer. *Cancer Res. Treatment*, **47**, 823–833.
24. Choi,S., Shin,J.H., Lee,Y.R., Joo,H.K., Song,K.H., Na,Y.G., Chang,S.J., Lim,J.S. and Jeon,B.H. (2016) Urinary APE1/Ref-1: a potential bladder cancer biomarker. *Dis. Markers*, **2016**, 7276502.
25. Cao,L., Cheng,H., Jiang,Q., Li,H. and Wu,Z. (2020) APEX1 is a novel diagnostic and prognostic biomarker for hepatocellular carcinoma. *Aging (Albany NY)*, **12**, 4573–4591.
26. Abbotts,R. and Madhusudan,S. (2010) Human AP endonuclease 1 (APE1): from mechanistic insights to druggable target in cancer. *Cancer Treat. Rev.*, **36**, 425–435.
27. Thakur,S., Sarkar,B., Cholia,R.P., Gautam,N., Dhiman,M. and Mantha,A.K. (2014) APE1/Ref-1 as an emerging therapeutic target for various human diseases: phytochemical modulation of its functions. *Exp. Mol. Med.*, **46**, e106.
28. Choi,S., Joo,H.K. and Jeon,B.H. (2016) Dynamic regulation of APE1/Ref-1 as a therapeutic target protein. *Chonnam Med J*, **52**, 75–80.
29. Kelley,M.R., Cheng,L., Foster,R., Tritt,R., Jiang,J., Broshears,J. and Koch,M. (2001) Elevated and altered expression of the multifunctional DNA base excision repair and redox enzyme Ape1/ref-1 in prostate cancer. *Clin. Cancer Res.*, **7**, 824–830.
30. Woo,J., Park,H., Sung,S.H., Moon,B.I., Suh,H. and Lim,W. (2014) Prognostic value of human apurinic/apyrimidinic endonuclease 1 (APE1) expression in breast cancer. *PLoS One*, **9**, e99528.
31. Qing,Y., Li,Q., Ren,T., Xia,W., Peng,Y., Liu,G.L., Luo,H., Yang,Y.X., Dai,X.Y., Zhou,S.F. *et al.* (2015) Upregulation of PD-L1 and APE1 is associated with tumorigenesis and poor prognosis of gastric cancer. *Drug Des Devel Ther*, **9**, 901–909.
32. Kaneda,K., Sekiguchi,J. and Shida,T. (2006) Role of the tryptophan residue in the vicinity of the catalytic center of exonuclease III family AP endonucleases: AP site recognition mechanism. *Nucleic Acids Res.*, **34**, 1552–1563.
33. Khanam,T., Shukla,A., Rai,N. and Ramachandran,R. (2015) Critical determinants for substrate recognition and catalysis in the m. tuberculosis class II AP-endonuclease/3′-5′ exonuclease III. *Biochim. Biophys. Acta - Proteins Proteomics*, **1854**, 505–516.
34. Redrejo-Rodríguez,M., Vigouroux,A., Mursalimov,A., Grin,I., Alili,D., Koshenov,Z., Akishev,Z., Maksimenko,A., Bissenbaev,A.K., Matkarimov,B.T. *et al.* (2016) Structural comparison of AP endonucleases from the exonuclease III family reveals new amino acid residues in human AP endonuclease 1 that are involved in incision of damaged DNA. *Biochimie*, **128-129**, 20–33.
35. Aslanidis,C. and de Jong,P.J. (1990) Ligation-independent cloning of PCR products (LIC-PCR). *Nucleic Acids Res.*, **18**, 6069–6074.
36. Roy,R., Hohng,S. and Ha,T. (2008) A practical guide to single-molecule FRET. *Nat. Methods*, **5**, 507–516.
37. Selvin,P.R. and Ha,T. (2008) In: *Single-Molecule Techniques: A Laboratory Manual*. 1st edn. Cold Spring Harbor Laboratory Press.
38. Roy,R., Kozlov,A.G., Lohman,T.M. and Ha,T. (2007) Dynamic structural rearrangements between DNA binding modes of e. coli SSB protein. *J. Mol. Biol.*, **369**, 1244–1257.

39. Humphrey,W., Dalke,A. and Schulten,K. (1996) VMD: visual molecular dynamics. *J. Mol. Graph.*, **14**, 33–38.
40. Goddard,T.D., Huang,C.C., Meng,E.C., Pettersen,E.F., Couch,G.S., Morris,J.H. and Ferrin,T.E. (2018) UCSF chimerax: meeting modern challenges in visualization and analysis. *Protein Sci.*, **27**, 14–25.
41. Pettersen,E.F., Goddard,T.D., Huang,C.C., Meng,E.C., Couch,G.S., Croll,T.I., Morris,J.H. and Ferrin,T.E. (2021) UCSF chimerax: structure visualization for researchers, educators, and developers. *Protein Sci.*, **30**, 70–82.
42. Shida,T., Noda,M. and Sekiguchi,J. (1996) Cleavage of single- and double-stranded DNAs containing an abasic residue by escherichia coli exonuclease III (AP endonuclease VI). *Nucleic Acids Res.*, **24**, 4572–4576.
43. Chawla,M., Chermak,E., Zhang,Q., Bujnicki,J.M., Oliva,R. and Cavallo,L. (2017) Occurrence and stability of lone pair-π stacking interactions between ribose and nucleobases in functional RNAs. *Nucleic Acids Res.*, **45**, 11019–11032.
44. Henikoff,S. (1984) Unidirectional digestion with exonuclease III creates targeted breakpoints for DNA sequencing. *Gene*, **28**, 351–359.
45. Shida,T., Kaneda,K., Ogawa,T. and Sekiguchi,J. (1999) Abasic site recognition mechanism by the *Escherichia coli* exonuclease III. *Nucleic Acids Symp. Ser.*, **42** , 195–196.
46. Theile,C.S., Witte,M.D., Blom,A.E.M., Kundrat,L., Ploegh,H.L. and Guimaraes,C.P. (2013) Site-specific N-terminal labeling of proteins using sortase-mediated reactions. *Nat. Protoc.*, **8**, 1800–1807.
47. Myong,S., Cui,S., Cornish,P.V., Kirchhofer,A., Gack,M.U., Jung,J.U., Hopfner,K.P. and Ha,T. (2009) Cytosolic viral sensor RIG-I is a 5′-Triphosphate-Dependent translocase on double-stranded RNA. *Science*, **323**, 1070–1074.
48. Ding,Y., Li,X., Zhang,X., Li,F., Hou,X. and Wu,P. (2019) Systematic probing of the sequence selectivity of exonuclease III with a photosensitization colorimetric assay. *ACS Omega*, **4**, 13382–13387.
49. Linxweiler,W. and Hörz,W. (1982) Sequence specificity of exonuclease III from e. coli. *Nucleic Acids Res.*, **10**, 4845–4859.